As-Prepared Single-Crystalline Hematite Rhombohedra and Subsequent Conversion into Monodisperse Aggregates of Magnetic Nanocomposites of Iron and Magnetite

Tae-Jin Park[†] and Stanislaus S. Wong*[,†,‡]

Department of Chemistry, State University of New York at Stony Brook, Stony Brook, New York 11794-3400, and Materials and Chemical Sciences Department, Brookhaven National Laboratory, Building 480, Upton, New York 11973

Received June 29, 2006

Monodisperse nanocrystalline rhombohedral composites of Fe and Fe_3O_4 magnetic materials have been obtained employing a reduction reaction, in a flowing gas mixture of H_2 and N_2, of single-crystalline, submicron-sized α-Fe_2O_3 rhombohedral precursors. This synthesis is significant in that we were able to create a nanocomposite with hard and soft magnetic phases juxtaposed within one discrete, anisotropic structure. In turn, the precursor hematite rhombohedra of reproducible shape were successfully prepared using a facile, environmentally friendly, large-scale molten-salt reaction. Rhombohedra represent a high-surface-area, anisotropic formulation of an industrially important material (iron oxide), which is an active component of gas sensors, photocatalysts, and other types of catalytic materials. Moreover, the predictive formation of these materials has been investigated through a systematic variation of experimental parameters. Extensive structural characterization of as-prepared samples has been performed using scanning electron microscopy, transmission electron microscopy (TEM), high-resolution TEM, energy-dispersive X-ray spectroscopy, selected area electron diffraction, X-ray diffraction, and superconducting quantum interference device (SQUID) magnetic measurements.

Introduction

Monodisperse inorganic mesoscopic structures with well-defined size, shape, chemical composition, and crystallinity have attracted extensive synthetic attention because of their novel morphology-dependent properties and their relevant applications including but not limited to biosensing, catalysis, optics, and data storage.[1−8] In particular, the generation of nanostructured magnetic materials with controllable shape and size in large quantities is of significant importance due to the potential applications, ranging from ferrofluids, advanced magnetic materials, catalysts, colored pigments, and high-density magnetic recording media to medical diagnostic equipment.[9] Much of the existing research though has focused on the synthesis and morphological organization of phase-pure nanosized building blocks such as nanoparticles. The fabrication of nanosized composites, such as core−shell, coaxial cable as well as one and two-dimensional structures, has not been investigated as comprehensively.[10−17] Among magnetic materials, the Fe/Fe_3O_4 composite system has specifically attracted considerable attention due to its favorable magnetoelectric and transport (including high conductivity) properties.[18−21] Moreover, this composite has been shown to produce a novel and active heterogeneous Fenton system, important in the oxidation of organic contaminants.[22]

Most of the synthetic routes associated with composite formation follow a "bottom up" strategy, wherein growth

* To whom correspondence should be addressed. Phone: (631)632-1703. E-mail: sswong@notes.cc.sunysb.edu.
[†] State University of New York at Stony Brook.
[‡] Brookhaven National Laboratory.

(1) Alivisatos, A. P. *Science* **1996**, *271*, 933.
(2) Ahmadi, T. S.; Wang, Z. L.; Green, T. C.; Henglein, A.; El-Sayed, M. A. *Science* **1996**, *272*, 1924.
(3) Cui, Y.; Lieber, C., M. *Science* **2001**, *291*, 851.
(4) Sun, Y.; Xia, Y. *Science* **2002**, *298*, 2176.
(5) Sun, S.; Murray, C. B.; Weller, D.; Folks, L.; Moser, A. *Science* **2000**, *287*, 1989.
(6) Bruchez, M.; Moronne, M.; Gin, P.; Weiss, S.; Alivisatos, A. P. *Science* **1998**, *281*, 2013.
(7) Wang, J.; Gudiksen, M. S.; Duan, X.; Cui, Y.; Lieber, C., M. *Science* **2001**, *293*, 1455.
(8) Xia, Y.; Yang, P.; Sun, Y.; Wu, Y.; Mayers, B.; Gates, B.; Yin, Y.; Kim, F.; Yan, H. *Adv. Mater.* **2003**, *15*, 353.
(9) Hyeon, T. *Chem. Commun.* **2003**, 927.
(10) Yang, H. G.; Zeng, H. C. *J. Am. Chem. Soc.* **2005**, *127*, 270.
(11) Park, J.; Lee, E.; Hwang, N.-M.; Kang, M.; Kim, S. C.; Hwang, Y.; Park, J.-G.; Noh, H.-J.; Kim, J.-Y.; Park, J.-H.; Hyeon, T. *Angew. Chem., Int. Ed.* **2005**, *44*, 2.
(12) Liu, Z.; Zhang, D.; Han, S.; Li, C.; Lei, B.; Lu, W.; Fang, J.; Zhou, C. *J. Am. Chem. Soc.* **2005**, *127*, 6.
(13) Kim, B.-S.; Qiu, J.-M.; Wang, J.-P.; Taton, T. A. *Nano Lett.* **2005**, *5*, 1987.
(14) Zhang, D.-F.; Sun, L.-D.; Jia, C.-J.; Yan, Z.-G.; You, L.-P.; Yan, C.-H. *J. Am. Chem. Soc.* **2005**, *127*, 13492.
(15) Tzitzios, V.; Niarchos, D.; Hadjipanayis, G.; Devlin, E.; Petridis, D. *Adv. Mater.* **2005**, *17*, 2188.
(16) Zeng, H.; Li, J.; Wang, Z. L.; Liu, J. P.; Sun, S. *Nano Lett.* **2004**, *4*, 187.
(17) Teng, X.; Yang, H. *J. Am. Chem. Soc.* **2003**, *125*, 14559.
(18) Yang, J. B.; Malik, S. K.; Zhou, X. D.; Kim, M. S.; Yelon, W. B.; James, W. J.; Anderson, H. U. *J. Phys. D:* Appl. Phys. **2005**, *38*, 1215.
(19) Zeng, H.; Li, J.; Liu, J. P.; Wang, Z. L.; Sun, S. *Nature* **2002**, *420*, 395.
(20) Bonetti, E.; Del Bianco, L.; Signoretti, S.; Tiberto, P. *J. Appl. Phys.* **2001**, *89*, 1806.
(21) Ding, J.; Miao, W. F.; Street, R.; McCormick, P. G. *Scr. Mater.* **1996**, *35*, 1307.
(22) Moura, F. C. C.; Araujo, M. H.; Costa, R. C. C.; Fabris, J. D.; Ardisson, J. D.; Macedo, W. A. A.; Lago, R. M. *Chemosphere* **2005**, *60*, 1118.

10.1021/cm061503s CCC: $33.50 © 2006 American Chemical Society
Published on Web 10/07/2006

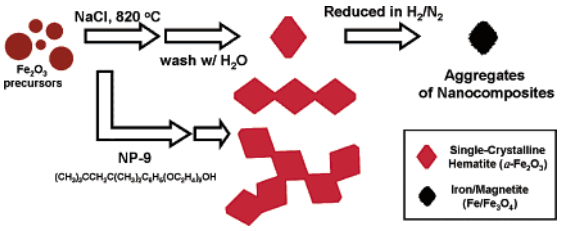

Figure 1. Schematic illustration of the generation of single-crystalline hematite rhombohedra (as well as other hematite structural motifs) and corresponding Fe/Fe_3O_4 nanocomposites.

of the resulting structure occurs through assembly of constituent molecular species. By contrast, in our approach (Figure 1), we were able to transform as-prepared hematite rhombohedra into nanocomposites of Fe and Fe_3O_4 by reducing hematite (α-Fe_2O_3) nanocrystals in the presence of a gaseous mixture of 5% H_2 in N_2.[23−27] That is, our particular strategy in composite formation was to initiate in situ, localized chemical transformations of precursor particles. Practically speaking, we were able to reduce the surface of hematite rhombohedra to an iron/magnetite composite with a corresponding color change of the sample from a reddish hue of the initial precursor to the deep black of the resulting product.

We demonstrate our multi-step synthesis through the initial production of a hematite precursor, a single-crystalline rhombohedral crystal with the corundum structure, which has been previously difficult to synthesize. Hematite is thought to be catalytic in the oxidation of chlorinated pollutants in groundwater and is found in the clay fraction of tropical and sub-tropical soils, giving them their pink−bright red hue. Bacteria in surface waters are known to catalyze the oxidation of magnetite (Fe_3O_4) to hematite.[28] Because of its high stability, relatively low cost, and *n*-type semiconducting properties with a small band gap (2.1 eV), α-Fe_2O_3 has been associated with applications ranging from gas sensing, catalysis, and solar energy conversion to pigmentation.[29−31] Specifically, the synthesis of rhombohedral hematite is a significant advance in nanoparticle chemistry not only because this particular morphology is a rarely observed structural motif of this material but also because this work represents the large-scale generation of a high-surface-area formulation of an industrially important material (iron oxide).

Considerable efforts have been expended in the generation of nanoscale structures of hematite, using a variety of techniques such as chemical precipitation, sol−gel techniques, hydrothermal approaches, forced hydrolysis, and solid-state reaction, to name a representative few.[23,32−50] However, most of the aforementioned solution-phase approaches tend to involve the use of organometallic precursors, surfactants, and solvents in either potentially hazardous or rather complicated protocols. It is therefore of interest to develop an environmentally friendly and efficient methodology to synthesize iron oxides. We have been particularly interested in exploring the use of molten-salt, solid-state reactions, due to their relative environmental friendliness, simplicity, relative nontoxicity, facility of use, and versatility as practical, generalizable, large-scale approaches to generating single-crystalline metal oxide nanomaterials.[51−55] In these reactions, since the nature of the net products strongly depends on the structural and chemical nature of the initial iron precursors, one of the main challenges of applying molten-salt methods to the production of hematite has been the development of reproducible control over the size, shape, and crystallinity of the resulting structures.[56] Though this need for reliable control explains our strong motivation for generating hematite rhombohedra, there are other fundamental reasons for doing so.

It has been found that the shape of a nanoparticle, which determines the exposed crystallographic surface (and its corresponding surface energy) enclosing the particle, can have a dramatic effect on its properties. As examples, the relative intensities of X-ray diffraction peaks, the positions

(23) Wang, H.; Zhang, X.; Liu, B.; Zhao, H.; Li, Y.; Huang, Y.; Du, Z. *Chem. Lett.* **2005**, *34*, 184.
(24) Zhao, W.; Gu, J.; Zhang, L.; Chen, H.; Shi, J. *J. Am. Chem. Soc.* **2005**, *127*, 8916.
(25) Jia, C.-J.; Sun, L.-D.; Yan, Z.-G.; You, L.-P.; Luo, F.; Han, X.-D.; Pang, Y.-C.; Zhang, Z.; Yan, C.-H. *Angew. Chem., Int. Ed.* **2005**, *44*, 4328.
(26) Ohmori, M.; Matijevic, E. *J. Colloid Interface Sci.* **1993**, *160*, 288.
(27) Brahma, P.; Banerjee, S.; Das, D.; Mukhopadhyay, P. K.; Chatterjee, S.; Nigam, A. K.; Chakravorty, D. *J. Magn. Magn. Mater.* **2002**, *246*, 162.
(28) Brown, D. A.; Sherriff, B. L.; Sawicki, J. A. *Geochim. Cosmochim. Acta* **1997**, *61*, 3341.
(29) Chen, J.; Xu, L.; Li, W.; Gou, X. *Adv. Mater.* **2005**, *17*, 582.
(30) Gondal, M. A.; Hameed, A.; Yamani, Z. H.; Suwaiyan, A. *Chem. Phys. Lett.* **2004**, *385*, 111.
(31) Ohmori, T.; Takahashi, H.; Mametsuka, H.; Suzuki, E. *Phys. Chem. Chem. Phys.* **2000**, *2*, 3519.
(32) Matijevic, E. *Chem. Mater.* **1993**, *5*, 412.
(33) Ocana, M.; Rodriguez-Clemente, R.; Serna, C. J. *Adv. Mater.* **1995**, *7*, 212.
(34) Wong, S. S.; Brus, L. E. *J. Phys. Chem. B* **2001**, *105*, 599.
(35) Frandsen, C.; Morup, S. *Phys. Rev. Lett.* **2005**, *94*, 027202.
(36) Jin, J.; Ohkoshi, S.-i.; Hashimoto, K. *Adv. Mater.* **2004**, *16*, 48.
(37) Woo, K.; Lee, H. J.; Ahn, J.-P.; Park, Y. S. *Adv. Mater.* **2003**, *15*, 1761.
(38) Dong, W.; Zhu, C. *J. Mater. Chem.* **2002**, *12*, 1676.
(39) Sugimoto, T.; Wang, Y.; Itoh, H.; Muramatsu, A. *Colloids Surf. A* **1998**, *134*, 265.
(40) Jing, Z.; Han, D.; Wu, S. *Mater. Lett.* **2005**, *59*, 804.
(41) Wang, X.; Chen, X.; Gao, L.; Zheng, H.; Ji, M.; Tang, C.; Shen, T.; Zhang, Z. *J. Mater. Chem.* **2004**, *14*, 905.
(42) Jones, F.; Ogden, M. I.; Oliveira, A.; Parkinson, G. M.; Richmond, W. R. *CrystEngComm* **2003**, *5*, 159.
(43) Raming, T. P.; Winnubst, A. J. A.; van Kats, C. M.; Philipse, A. P. *J. Colloid Interface Sci.* **2002**, *249*, 346.
(44) Chen, L. X.; Liu, T.; Thurnauer, M. C.; Csencsits, R.; Rajh, T. *J. Phys. Chem. B* **2002**, *106*, 8539.
(45) Hansen, M. F.; Koch, C. B.; Morup, S. *Phys. Rev. B* **2000**, *62*, 1124.
(46) Zboril, R.; Mashlan, M.; Barcova, K.; Vujtek, M. *Hyp. Interact.* **2002**, *139/140*, 597.
(47) Xu, X. N.; Wolfus, Y.; Shaulov, A.; Yeshurun, Y.; Felner, I.; Nowik, I.; Kotypin, Y.; Gedanken, A. *J. Appl. Phys.* **2002**, *91*, 4611.
(48) Zysler, R. D.; Vasquez-Mansilla, M.; Arciprete, C.; Dimitrijewits, M.; Rodriguez-Sierra, D.; Saragovi, C. *J. Magn. Magn. Mater.* **2001**, *224*, 39.
(49) Shen, X.-P.; Liu, H.-J.; Pan, L.; Chen, K.-M.; Hong, J.-M.; Xu, Z. *Chem. Lett.* **2004**, *33*, 1128.
(50) Fu, Y. Y.; Wang, R. M.; Xu, J.; Chen, J.; Yan, Y.; Narlikar, A. V.; Zhang, H. *Chem. Phys. Lett.* **2003**, *379*, 373.
(51) Park, T.-J.; Mao, Y.; Wong, S. S. *Chem. Commun.* **2004**, 2078.
(52) Park, T.-J.; Papaefthymiou, G. C.; Moodenbaugh, A. R.; Mao, Y.; Wong, S. S. *J. Mater. Chem.* **2005**, *15*, 2099.
(53) Mao, Y.; Banerjee, S.; Wong, S. S. *J. Am. Chem. Soc.* **2003**, *125*, 15718.
(54) Mao, Y.; Wong, S. S. *J. Am. Chem. Soc.* **2004**, *126*, 15245.
(55) Mao, Y.; Park, T.-J.; Wong, S. S. *Chem. Commun.* **2005**, 5721.
(56) Zboril, R.; Mashlan, M.; Petridis, D. *Chem. Mater.* **2002**, *14*, 969.

of bands in optical spectra, and the magnitude of sublimation energies of a wide variety of materials including Au and Ag_2S are intrinsically coupled with particle morphology (such as icosahedra, cubes, and tetrahedra).[57−59] With hematite in particular, changes in microhardness, electrical conductivity (i.e. mobility enhancement), and superparamagnetic blocking behavior are strongly associated with its physical and structural characteristics.[48,60,61] As another relevant manifestation of the significance of shape, for magnetic nanoparticles in particular such as the Fe/Fe_3O_4 composite synthesized herein, shape anisotropy and crystalline anisotropy are expected to have a profound influence on their intrinsic magnetic properties (such as coercivity).[9] In fact, the magnetic anisotropy (i.e., higher coercivity) present in rod-shaped magnetic particles, which by contrast is not observed in symmetrically shaped spheres or cubes, has been exploited in the use of these acicular particles for commercial magnetic recording media.[9]

In the experiments reported herein, we were able to generate distinctive structural polymorphs of hematite iron oxide from relatively polydisperse, commercially available starting precursor materials. We were subsequently able to transform these single-crystalline α-Fe_2O_3 rhombohedral structures into their magnetic nanocrystalline composite counterparts, Fe/Fe_3O_4. These samples were characterized by a number of techniques, including scanning electron microscopy (SEM), transmission electron microscopy (TEM), high-resolution TEM (HRTEM), energy-dispersive X-ray spectroscopy (EDS), selected area electron diffraction (SAED), X-ray diffraction (XRD), and superconducting quantum interference device (SQUID) measurements.

Experimental Section

General. Specifically, commercial iron(III) oxide or Fe_2O_3 (Aldrich, polydisperse nanopowder), NP-9 surfactant (Aldrich, polyoxyethylene(9)nonylphenyl ether), and NaCl (Mallinckrodt, sodium chloride) were used as supplied. The choice of the surfactant was governed by its prior versatility in the preparation of elongated structures of metal oxides, its relative nontoxicity, and comparative facility of use.[52] Stoichiometric amounts of Fe_2O_3, NaCl, and NP-9 were mixed (in molar ratios of 1:40:6, 2:40:6, 3:40:6, and 6:40:6, respectively, for the generation of varying structural motifs of hematite), thoroughly ground in an agate mortar, and subsequently sonicated.

In a typical synthesis of submicron-sized, single-crystalline α-Fe_2O_3 rhombohedra, 0.5 and 20 mmol of Fe_2O_3 and NaCl, respectively, were mixed thoroughly in an agate mortar. For elongated α-Fe_2O_3 structures, 1, 1.5, and 3 mmol of Fe_2O_3 along with 20 mmol of NaCl, respectively, were meticulously mixed, after which 2 mL of NP-9 was subsequently added. The resulting mixture was ground for at least 30 min prior to sonication for an additional 5 min. Identical procedures were employed for samples containing different molar ratios of initial precursors. The resulting mixture was then placed in a ceramic crucible, inserted into a quartz tube, heated at a ramp rate of 5°C per min up to an annealing temperature at 820 °C for 3.5 h, and cooled thereafter to room temperature. As-prepared material was subsequently washed several times with distilled water, collected by centrifugation, and dried at 120 °C in a drying oven.

Hematite rhombohedra were converted to their magnetic analogues (i.e., composites of Fe/Fe_3O_4) through a reduction reaction in a flowing gaseous mixture. Briefly, the as-prepared hematite product was heated in a tube furnace at 360 °C for 5 h under a continuous flow of 5% H_2 in N_2. After the gas flow was stopped, the resulting product was subsequently heated to 240 °C for 2 h, cooled to room temperature, and then collected without further treatment.

X-ray Diffraction. Crystallographic information of as-prepared samples was obtained on a Scintag diffractometer, operating in the Bragg configuration using Cu Kα radiation ($\lambda = 1.54$ Å). Powder XRD samples were prepared by grinding products thoroughly in ethanol using a mortar and pestle, followed by loading onto glass slides, and subsequent drying in air. Diffraction patterns were collected from 10 to 80° at a scanning rate of 2°/min with a step size of 0.02°. Parameters used for slit widths and accelerating voltage were identical for all samples.

Electron Microscopy. The particle size and morphology of the resulting Fe_2O_3 as well as Fe/Fe_3O_4 products were initially characterized using a field emission scanning electron microscopy (SEM, Leo 1550) operated at accelerating voltages of 15 kV and equipped with EDS capabilities. Specifically, samples were deposited onto a Si wafer, which were then attached to the surface of SEM brass stubs using a copper tape. These samples were then conductively coated with gold by sputtering them for 10−20 s to minimize charging effects under SEM imaging conditions.

Specimens for TEM and HRTEM were obtained by drying sample droplets from an ethanolic dispersion onto a 300 mesh Cu grid coated with a lacey carbon film. Low magnification TEM images were taken at an accelerating voltage of 120 kV on a Philip CM12 instrument. High-resolution images were obtained on a JEOL 2010F HRTEM at an accelerating voltage of 200 kV. This instrument was equipped with an Oxford INCA EDS system with the potential of performing SAED to further characterize individual iron oxide nanostructures.

SQUID. Magnetization measurements were obtained using an MPMS magnetometer. Powder samples of as-prepared products were pressed lightly, then loaded into a gel cap, and covered with silica wool. This was held within a uniform drinking straw, which was attached to the sample rod of the MPMS apparatus. Signals generated by measurements of an empty sample holder demonstrated that the holder assembly contributes <1% to the overall magnetic signal.

Results and Discussion

Iron Oxide Rhombohedra. The purity and crystallinity of as-prepared hematite (α-Fe_2O_3) structures were examined using powder XRD measurements (Figure 2). It is evident that the observed pattern of the collected powder displayed all of the expected peaks emanating from the α-Fe_2O_3 structure with very few, if any, impurity peaks. In effect, diffraction peaks in Figure 2A can be indexed to the rhombohedral structure of α-Fe_2O_3 [space group: R_{-3c}] with structural parameters of $a = b = 5.038$ Å, $c = 13.772$ Å, $\alpha = \beta = 90°$, and $\gamma = 120°$, which are in good agreement with literature results (i.e., JCPDS 33-0664, Figure 2B).

(57) Kim, F.; Connor, S.; Song, H.; Kuykendall, T.; Yang, P. *Angew. Chem., Int. Ed.* **2004**, *43*, 3673.
(58) Lim, W. P.; Zhang, Z.; Low, H. Y.; Chin, W. S. *Angew. Chem., Int. Ed.* **2004**, *43*, 5685.
(59) Tanigaki, T.; Suzuki, H.; Kimura, Y.; Kaito, C.; Saito, Y. *Surf. Rev. Lett.* **2003**, *10*, 455.
(60) Stevenson, M. E.; Kaji, M.; Bradt, R. C. *J. Eur. Ceram. Soc.* **2002**, *22*, 1137.
(61) Miller, E. L.; Paluselli, D.; Marsen, B.; Rocheleau, R. E. *Thin Solid Films* **2004**, *466*, 307.

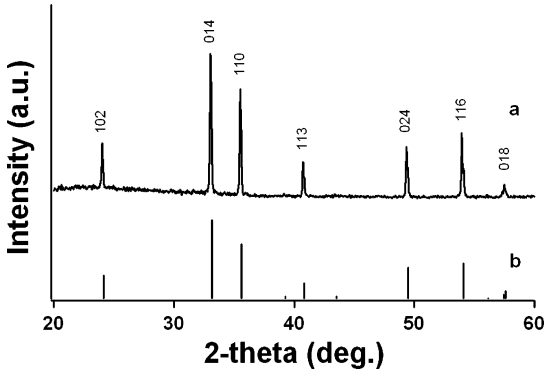

Figure 2. XRD patterns of as-prepared α-Fe_2O_3 rhombohedral particles (a) and of α-Fe_2O_3 from the JCPDS 33-0664 database standard (b).

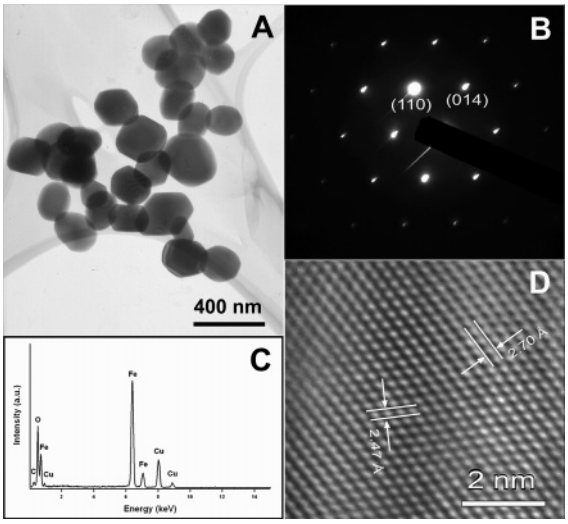

Figure 3. (A) TEM image of as-prepared α-Fe_2O_3 rhombohedral particles. (B) SAED pattern of an α-Fe_2O_3 rhombohedron. (C) EDS of an α-Fe_2O_3 rhombohedron. The Cu and C peaks originate from the TEM grid. (D) HRTEM image of a typical portion of an α-Fe_2O_3 rhombohedron.

A typical TEM image of α-Fe_2O_3 rhombohedra, generated from the current molten-salt method with a 1:40 molar ratio of Fe_2O_3 to NaCl, is shown in Figure 3A. The size of the particles, which can be described in terms of the mean lengths of the shorter and longer diagonals of the rhombohedron, were measured to be 231 ± 40 and 198 ± 35 nm, respectively, with their aspect ratio calculated to be 1.2 on average. SAED data taken from an individual rhombohedral structure (Figure 3B) show the presence of sharp diffraction spots indicating the formation of well-developed, single-crystalline hematite particles. We note that the electron diffraction patterns obtained from different positions along the same rhombohedron as well as from different rhombohedra also show similar sharp diffraction spots. To confirm the chemical composition of the as-prepared structures, EDS spectra (Figure 3C) were taken at a number of selected positions of the sample. The elemental signatures obtained are identical within experimental accuracy, and essentially Fe and O were observed, as expected. The Cu and C signals arise from the TEM grid. In Figure 3D, a HRTEM image obtained from part of an individual α-Fe_2O_3 rhombohedron is displayed so as to further confirm the single-crystalline nature of our as-prepared structures. This image shows a typical crystalline domain with interplanar spacings of about 2.70 and 2.47 Å, which are comparable with the literature values of 2.700 and 2.519 Å, which correspond to the (014) and (110) planes of the hexagonal phases of the α-Fe_2O_3 rhombohedral crystal, respectively (JCPDS 33-0664).

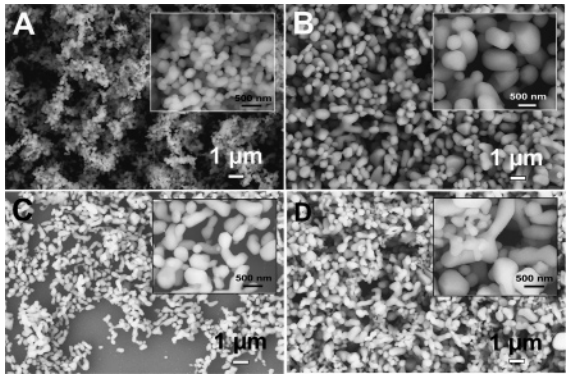

Figure 4. SEM images of α-Fe_2O_3 structures prepared using a molten salt method with 1:40 (A), 2:40 (B), 3:40 (C), and 6:40 (D) molar ratios of Fe_2O_3 to NaCl precursors, respectively. For the purpose of shape control, the precursors in panels B, C, and D were added to 2 mL of NP-9, a nonionic surfactant. Insets show higher-magnification images of individual hematite particles.

Figure 4 shows SEM images revealing the morphologies of as-prepared α-Fe_2O_3 structures, generated from the as-described protocol. It can be observed that the α-Fe_2O_3 product, prepared using a molten salt method with a 1:40 molar ratio of Fe_2O_3 to NaCl, mainly consists of discrete rhombohedral structures with smooth surfaces (Figure 4A). The size of the particulates is consistent with that from the TEM data discussed above. It can also be observed that the faces of the α-Fe_2O_3 rhombohedra are essentially flat though some of the corners of these structures are slightly truncated.

To obtain further insight into the formation of different shapes of the α-Fe_2O_3 structures, the morphologies of α-Fe_2O_3 structures generated from the precursors, derived from 2:40:6, 3:40:6, and 6:40:6 (Fe_2O_3:NaCl:NP-9) molar ratios, are shown in Figure 4, panels B, C, and D, respectively. It can be observed that the shapes of α-Fe_2O_3 structures alter from their rhombohedral motifs into peanut-shaped structures. Moreover, the aspect ratio of these materials increases nonlinearly with higher molar ratios of Fe_2O_3 precursor to surfactant content in the system. In fact, for these molar ratios, the mean lengths of elongated α-Fe_2O_3 peanut-like structures are 1092 ± 389 (B), 1050 ± 183 (C), and 1611 ± 565 nm (D), respectively, and their mean widths (shorter side of each structure) measure 591 ± 108 (B), 329 ± 47 (C), and 476 ± 77 nm (D), respectively. Hence, their corresponding aspect ratios are 1.9, 3.3, and 3.5 for panels B, C, and D, respectively. The aspect ratio of 3.5, observed for the product in Figure 4D, is relatively smaller than expected. This value reflects the large degree of branching and higher overall polydispersity in the resultant iron oxide structures with increasing molar content of Fe_2O_3 and suggests the presence of numerous nucleation sites on the growing particles. Histograms of particle size (including lengths and widths) distributions for as-prepared hematite samples are shown in both Figure 5 and Supporting Information Figure S1.

To analyze the role of surfactant in this reaction, α-Fe_2O_3 products were prepared employing identical, as-reported experimental procedures in the absence of any surfactant.

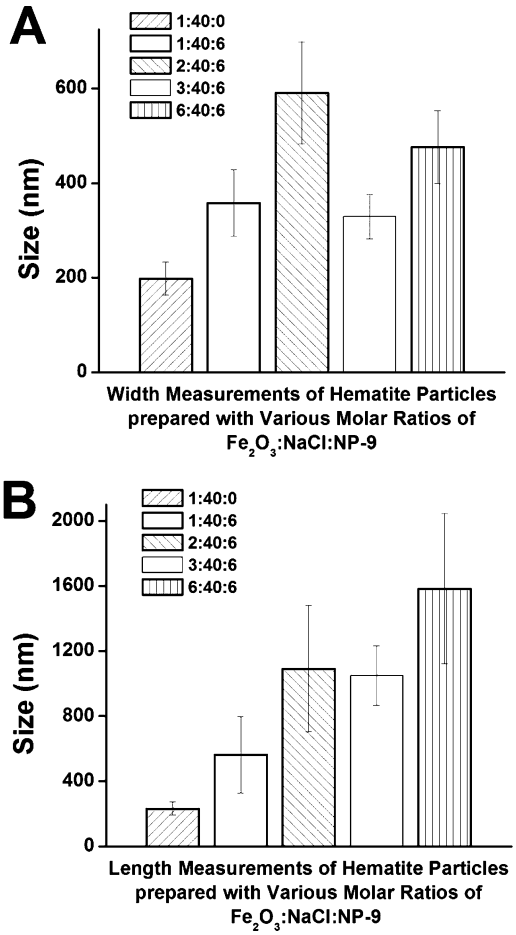

Figure 5. Histograms of size distributions of as-prepared hematite structures. Parameters for each structure are given in terms of width (A) and length (B). Molar ratios of reagents are given in the following order—Fe_2O_3:NaCl:NP-9 surfactant.

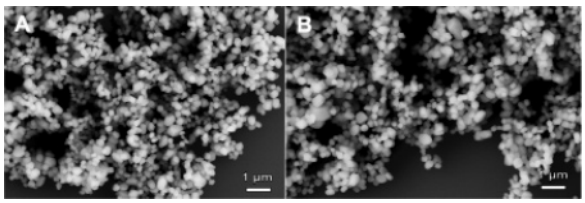

Figure 6. SEM images of α-Fe_2O_3 structures prepared from molar ratios of 3:40 (A) and 6:40 (B) of Fe_2O_3:NaCl precursors, without the presence of surfactant.

The morphologies of the resultant products generated from mixtures of (a) 3:40 and (b) 6:40 molar ratios of Fe_2O_3 to NaCl precursors, respectively, are shown in Figure 6. It is evident that all of these particles possess morphologies as well as size distributions that are consistent with the product, prepared with a molar ratio of Fe_2O_3 to NaCl precursors of 1:40 (Figures 4A and 5). Hence, it is apparent that surfactant, through its dispersing ability, can play a critical role adjusting the size and shape of these binary metal oxide particles. In fact, samples prepared from identical precursor ratios with and without surfactant suggest that the presence of surfactant will cause an elongation of the resulting products and skew their size distribution, as noted in Figure 5. For instance, SEM images of hematite prepared from a mixture of a 1:40 molar ratio of Fe_2O_3 to NaCl in the presence of NP-9 are shown in Supporting Information Figure S2; they are evidently more polydisperse in terms of size and shape. In

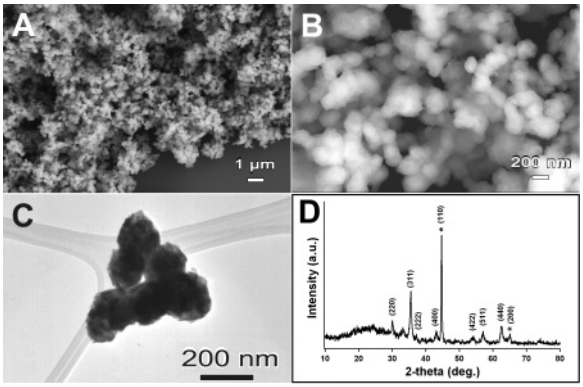

Figure 7. (A) Lower and (B) correspondingly higher magnification SEM image of as-transformed magnetic composites of Fe/Fe_3O_4. (C) TEM image of a cluster of individual Fe/Fe_3O_4 structures. (D) XRD pattern of as-transformed Fe/Fe_3O_4 structures. Asterisks indicate XRD peaks from Fe.

fact, SEM measurements indicate that hematite particles prepared from a molar ratio of Fe_2O_3:NaCl:NP-9 equal to 1:40:6 possess mean widths of 358 (± 70) nm and mean lengths of 562 (± 235) nm, with a measured aspect ratio of 1.6. Nevertheless, the single-crystalline nature of all of these surfactant-treated hematite particles (Figure 4, panels C and D) has been confirmed; associated TEM and SAED images are shown in Supporting Information Figure S3.

The observations described above confirm the significant role of the surfactant combined with other experimental parameters, such as the molar ratios of precursors and the addition of salt, to collectively yield single-crystalline α-Fe_2O_3 products with predictive control of size and shape. The presence of salt is expected to decrease the overall reaction temperature.[62] The liquid-like phase of the molten flux is expected to increase the mobility of its constituent components.

Fe/Fe_3O_4 Composites. The morphologies of the resulting Fe/Fe_3O_4 composites generated from the reduction reaction are shown in Figure 7, panels A and B. It can be observed that the size distribution, shape, and crystallinity of the resulting iron/magnetite composites are similar to those of their corresponding hematite precursors. For further comparison in their morphology, SEM images of rhombohedra of the hematite and the Fe/Fe_3O_4 composite are shown in Supporting Information Figure S4. We note that as-generated Fe/Fe_3O_4 structures possess somewhat roughened surfaces composed of multiple domains of iron and iron oxide (Figure 7C). We hypothesize that this morphological alteration can be attributed not only to differential rates of reduction with respect to the surface and bulk of the initial nanoparticle starting materials but also to the in situ formation of domains of elemental iron and magnetite. In fact, XRD data on the resulting composites of Fe and Fe_3O_4, derived from hematite precursors, in Figure 7D, display all of the expected peaks, in good agreement with literature results (Fe, JCPDS 06-0696; Fe_3O_4, JCPDS 19-0629), and confirm the expected chemical composition of the resulting composite Fe/Fe_3O_4 structure.

To further confirm the composition of our as-transformed magnetic materials, HRTEM has been performed on an

(62) Wiley, J. B.; Kaner, R. B. *Science* **1992**, *255*, 1093.

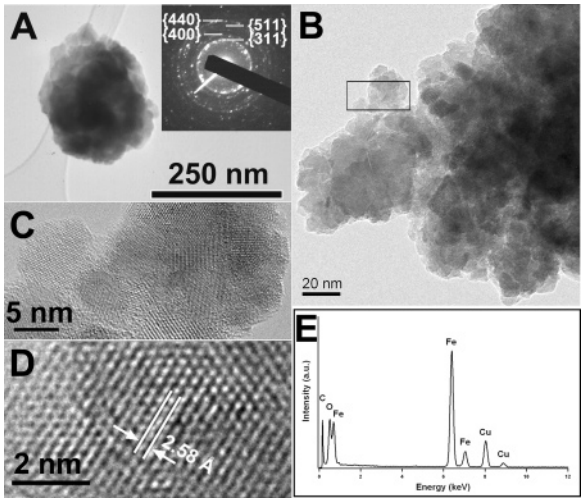

Figure 8. (A) TEM image of a typical individual magnetic composite of iron and magnetite. Inset shows the corresponding SAED pattern of an Fe/Fe_3O_4 rhombohedron. (B) Higher magnification image of the composite of Fe/Fe_3O_4. (C) Enlarged portion of the assembled nanostructure of Fe and Fe_3O_4, as delineated by the black square in (B). (D) HRTEM image of a typical lattice spacing of an Fe_3O_4 structure. (E) EDS spectra obtained from an individual Fe/Fe_3O_4 rhombohedron. The Cu and C peaks originate from the TEM grid.

individual Fe/Fe_3O_4 composite shown in Figure 8A. The SAED data taken of an individual rhombohedral structure (shown in the inset) show the presence of sharp diffraction spots and rings that could be assigned to that of Fe_3O_4. However, we note that the expected lattice spacing (2.0268 Å) of the {110} planes of Fe is very similar to the analogous lattice spacing (2.0993 Å) of the {400} planes of Fe_3O_4 and hence, these two distances are difficult to clearly differentiate between in the SAED pattern. Nevertheless, the electron diffraction patterns obtained from different areas of the composite structure also show similar results.

The higher magnification image of a typical Fe/Fe_3O_4 composite reveals that the surface of the rhombohedron is composed of multiple nanostructures with mean sizes of 11 ± 3 nm (Figure 8B). The nanostructures themselves are composed of multiple adjacent, discrete domain regions of Fe and Fe_3O_4 (Figure 8C). In Figure 8D, a HRTEM image obtained from a portion of an individual Fe/Fe_3O_4 composite is displayed so as to further confirm the single-crystalline nature of each individual domain of Fe and Fe_3O_4. This image shows a typical crystalline domain with an interplanar spacing of about 2.58 Å, comparable with the literature value of 2.532 Å, which corresponds to the {311} planes of the cubic phase of an Fe_3O_4 crystal (JCPDS #19-0629). To confirm the chemical composition of the as-prepared structures, EDS spectra (Figure 8E) were taken at a number of selected positions along the sample. The elemental signatures obtained are identical within experimental accuracy, and essentially only Fe and O were observed, as expected. We note that the relative intensity of oxygen for the Fe/Fe_3O_4 composite (Figure 8E) decreased slightly as compared with the data for the hematite precursor alone (Figure 3C), suggestive of a lowered oxygen density in the resulting composite structure, an observation consistent with a reduction reaction having occurred. The Cu and C signals arise from the TEM grid.

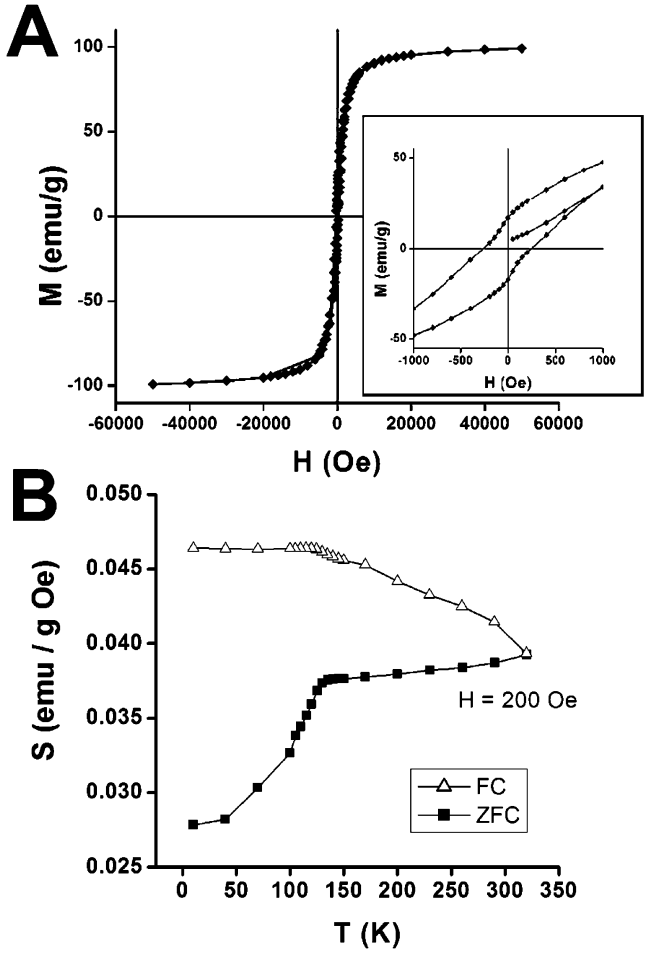

Figure 9. (A) Hysteresis loop at room temperature of as-transformed Fe/Fe_3O_4 composites. Inset shows the enlarged portion of the hysteresis loop revealing the coercivity of the Fe/Fe_3O_4 composite. (B) Temperature dependence of the magnetic susceptibility for Fe/Fe_3O_4 composite, showing zero field cooling (ZFC, closed circle) and field cooling (FC, closed square) curves, with an applied magnetic field set at 200 Oe.

Figure 9A shows the presence of a hysteresis loop at room temperature of the resultant nanocrystalline Fe/Fe_3O_4 composite magnetic material, revealing strong ferromagnetic behavior. These nanocomposites consist of magnetically hard and soft phases where there is some degree of magnetic exchange coupling between the Fe and magnetite domains. The magnetization curve shows a steep increase in magnetization with increasing field. The asymmetric shape of the hysteresis loop conveys two-phase behavior, implying that the dimension of the soft phase is smaller than that of the hard phase and that, furthermore, in this nanocomposite, the hard and soft phases are not able to completely switch cooperatively. Moreover, the kink at low field is related to the magnetization reversal of the soft magnetic phase, likely magnetite in this case.[19] The saturation magnetization (M_S: ~100 emu/g) measured for the Fe/Fe_3O_4 composite is about 20% higher than that for the magnetite phase and about 66% higher than the value of 60.1 emu/g observed for 11.5 nm-sized magnetite nanoparticles.[21,63,64] The additional 66% increase in M_S is consistent with and can be attributed to the presence of an extra 67% amount of Fe (as deduced from

(63) Maruyama, T.; Shinyashiki, Y. *Thin Solid Films* **1998**, *333*, 203.
(64) Goya, G. F.; Berquó, T. S.; Fonseca, F. C.; Morales, M. P. *J. Appl. Phys.* **2003**, *94*, 3520.

XRD analysis) in Fe/Fe_3O_4 nanocomposites. The structural inhomogeneity of the samples has a strong influence on the M_S value measured. In addition, the relatively high coercivity observed (H_C: 250 Oe) indicates the potential applicability of these nanoscale composite magnetic structures as low-cost hard magnetic materials. Our results are also comparable with data recently reported for similar structural analogues, having important applications in biomedical fields such as biomolecular separations, targeted drug delivery, cancer diagnosis and treatment, as well as magnetic resonance imaging.[24,65]

Figure 9B shows the magnetic susceptibility of these nanoscale composites as a function of temperature at an applied field strength of 200 Oe, after zero field cooling (ZFC) and also, with field cooling (FC). The curves show the presence of the Verwey transition[66] at a temperature of ~135 K, which is indicative of magnetite, arising from the ordering among Fe^{3+} and Fe^{2+} ions. The relatively higher Verwey transition temperature observed relative to pristine magnetite (~120 K) is consistent with values recently reported for similar Fe/Fe_3O_4 composite systems[18] and can be ascribed to the higher Fe content relative to that of Fe_3O_4. Hence, these results imply the potential usage of these materials in applications ranging from nanocomposite conductors to superconductors.[18]

Conclusions

The current work demonstrates the generation of monodisperse assemblies of rhombohedral nanocrystalline composites of Fe and Fe_3O_4 formed from a reordering of the microstructure of single-crystalline hematite rhombohedral precursors that occurred as a product of the reduction reaction in a gaseous mixture of 5% H_2 in N_2. The main significance of the work is that we were able to create a nanocomposite with hard and soft magnetic phases juxtaposed within one discrete, anisotropic structure. Nonetheless, this work is also relevant for other important reasons.

First, we have demonstrated our ability to prepare monodisperse hematite products with controlled size, shape, and monodispersity, starting from relatively inexpensive, commercially available polydisperse, polycrystalline, or amorphous precursors. Single-crystalline, monodisperse nanoscale α-Fe_2O_3 rhombohedra as well as elongated motifs of these materials are in fact an excellent model system to demonstrate this synthetic principle. This methodology allows for control over size, shape, and chemical composition of our as-prepared products using a simple, versatile, one-step, environmentally friendly, and large-scale solid-state chemical reaction in the presence of NaCl and a nonionic surfactant.

Second, rhombohedra represent a high-surface-area, anisotropic formulation of an industrially important material (iron oxide) that is an active component of gas sensors, photocatalysts, and other types of catalytic materials. Third, α-Fe_2O_3 hematite rhombohedra present themselves as a practical, low-cost chemical precursor material to the subsequent synthesis of magnetite. As previously alluded to, the development of a facile and economically viable synthetic strategy for the synthesis of hydrophilic, biocompatible magnetic particles (including magnetite) would benefit their technical use in biomedical fields, such as biomolecular separations, targeted drug delivery, tags for sensing and imaging, antitumor therapy, and magnetic resonance imaging.

The resulting Fe/Fe_3O_4 as well as α-Fe_2O_3 structures have been extensively characterized using a variety of microscopy, diffraction, spectroscopy, and SQUID results. As mentioned, nanostructured magnetic materials such as the composite described herein also have potential applications as ferrofluids, catalysts, colored pigments, and high-density magnetic recording media.[65] Hence, future research will focus on measurements (such as gas sensitivity, catalytic activity, and conductivity) of these as-generated structures to determine the net effect of shape and size on these intrinsic properties.

Acknowledgment. We acknowledge support of this work through the U.S. Department of Energy under Contract DE-AC02-98CH10886 for facility support, the National Science Foundation (CAREER Award DMR-0348239), and the donors of the American Chemical Society Petroleum Research Fund. Dr. James Quinn is acknowledged for his help with SEM and TEM results. Dr. Arnold R. Moodenbaugh is credited with the collection of SQUID data. We are also grateful to Dr. Yuanbing Mao (including for helpful discussions) and Prof. Jianyu Huang for their assistance with the HRTEM results.

Supporting Information Available: Four additional figures. This material is available free of charge via the Internet at http://pubs.acs.org.

CM061503S

(65) Deng, H.; Li, X.; Peng, Q.; Wang, X.; Chen, J.; Li, Y. *Angew. Chem., Int. Ed.* **2005**, *44*, 2782.
(66) Verwey, E. J. W. *Nature* **1939**, *144*, 327.